Evaluation of High-Frequency Induction Heat Sintering and Conventional Sintering in AlxCoCrFeMnNi High-Entropy Alloys

M.A. Ruiz-Esparza-Rodríguez, C.G. Garay-Reyes, J.M. Mendoza-Duarte, I. Estrada-Guel, J.L. Hernández-Rivera, J.J. Cruz-Rivera, E. Gutiérrez-Castañeda, S. González, A.M. Garay-Tapia, R. Martínez-Sánchez

PII: S0925-8388(22)01171-9

DOI: https://doi.org/10.1016/j.jallcom.2022.164780

Reference: JALCOM164780

To appear in: *Journal of Alloys and Compounds*

Received date: 22 November 2021
Revised date: 15 March 2022
Accepted date: 25 March 2022

Please cite this article as: M.A. Ruiz-Esparza-Rodríguez, C.G. Garay-Reyes, J.M. Mendoza-Duarte, I. Estrada-Guel, J.L. Hernández-Rivera, J.J. Cruz-Rivera, E. Gutiérrez-Castañeda, S. González, A.M. Garay-Tapia and R. Martínez-Sánchez, Evaluation of High-Frequency Induction Heat Sintering and Conventional Sintering in AlxCoCrFeMnNi High-Entropy Alloys,*Journal of Alloys and Compounds,* (2021) doi:https://doi.org/10.1016/j.jallcom.2022.164780

Evaluation of High-Frequency Induction Heat Sintering and Conventional Sintering in AlxCoCrFeMnNi High-Entropy Alloys

M.A. Ruiz-Esparza-Rodríguez[1], C.G. Garay-Reyes[1,*], J.M. Mendoza-Duarte[1], I. Estrada-Guel[1], J.L. Hernández-Rivera[2, 3], J.J. Cruz-Rivera[3], E. Gutiérrez-Castañeda[2, 3], S. González[4], A. M. Garay-Tapia[1] and R. Martínez-Sánchez[1,*]

[1] Centro de Investigación en Materiales Avanzados (CIMAV), Laboratorio Nacional de Nanotecnología, Miguel de Cervantes 120, 31136 Chihuahua, Chih., México.

[2] CONACYT - Instituto de Metalurgia, Universidad Autónoma de San Luis Potosí, Av. Sierra Leona 550, Lomas 2da Sección, 78210, San Luis Potosí, S.L.P, México

[3] Instituto de Metalurgia, Universidad Autónoma de San Luis Potosí, Av. Sierra Leona 550, Lomas 2da Sección, 78210, San Luis Potosí, S.L.P, México.

[4] Faculty of Engineering and Environment, Northumbria University, Newcastle upon Tyne NE1 8ST, UK.

*Corresponding authors e-mail: roberto.martinez@cimav.edu.mx, carlos.garay@cimav.edu.mx.

Abstract

$Al_xCoCrFeMnNi$ high-entropy alloys with different aluminum concentrations (x= 0.5, 1, and 1.5 at. %) were synthesized by mechanical alloying followed by consolidation using two different sintering methods, conventional (CS) and high-frequency induction heat + conventional (HFIHS + CS). The results show the presence of FCC, BCC, and $B2_{ordered}$ phases in all systems, regardless of the sintering method. The BCC phase exhibits morphological changes (cuboidal-type and plate-like) associated with the two sintering methods involving different diffusion rates and affecting the hardness values. The $M_{23}C_6$ carbide is identified in systems sintered by the CS method; meanwhile, the M_7C_3 carbide is identified in the HFIHS + CS method. Finally, the HFIHS + CS method results in a higher level of densification (~95%) than the CS method (~80%).

Keywords

High-Entropy Alloy; High-Frequency Induction Heat Sintering; Aluminum; Coarsening; Precipitation.

1. Introduction

Over the last decade, there has been increasing interest in studying the structure-mechanical property correlation of high-entropy alloys (HEAs) [1–3]. HEAs are alloys made out of five or more metallic elements with equiatomic or near equiatomic compositions, with concentrations from 5 to 35 at. % thus having a configurational entropy between 1.5R to 1.6R, where R is a universal constant [1, 4]. The chemical elements that constitute the HEAs, the processing methods, and the thermal treatments enable the tune of their crystalline structure and, therefore, the resulting properties [5, 6]. In this sense, phase transformations and their kinetics depend on the competition between entropy and enthalpy to minimize the Gibbs free energy [7, 8]. The first studies on HEA reported the formation of simple solid solutions (BCC, FCC and HCP). However, only some alloys satisfy the compositional requirement for simple solid solution formation. Most HEAs reported to date contain multiple phases and complex microstructures [9], including B2 + BCC phases and intermetallic phases, whose formation often competes with the formation of simple solid solution phases in HEAs [10].

The CoCrFeMnNi system is one of the most intensively studied among the numerous HEAs due to its physical properties and thermodynamic stability. It was first reported by Cantor et al. [11,12], and its microstructure consists of a single FCC solid solution. However, it has been reported that increasing the aluminum content in the CoCrFeMnNi system increases the proportion of the BCC and $B2_{ordered}$ phases [1, 12-15]. The $B2_{ordered}$ phase is the alloy matrix, while the BCC phase exhibits a cubic-type morphology, which originates via spinodal decomposition [12-15].

The formation of both BCC and $B2_{ordered}$ phases have been observed in equiatomic or non-equiatomic HEAs as major or minor phases [16, 17]. For example, Ma et al. [16-18] reported the presence of those phases in the $Al_2(NiCoFeCr)_{14}$ and $Al_xNiCoFeCr$ systems. They concluded that the morphology of the cuboidal-type

precipitates is attributed to lattice misfit ε between the matrix and the precipitates. They observed that a small ε (ε < 0.2 %) results in the formation of spherical/ellipsoidal-type precipitates. A moderate ε (ε ~ 0.4%) generates cuboidal-type precipitates while large ε (ε > 0.6 %) induces the formation of a weave-like microstructure. Regarding the $B2_{ordered}$ phase becomes the primary phase for aluminum additions greater than 10 at. % [16-19], and it is generally observed in alloys containing Fe, Co, Ni and Al upon heat treatment [20-23].

On the other hand, a subsequent sintering treatment step is required when HEAs are fabricated via powder metallurgy. The most common processes for sintering HEAs are spark plasma sintering (SPS), conventional sintering (CS) and hot isostatic pressing [24-28]. An alternative method that has been scarcely explored but is of great potential interest is High-Frequency Induction Heat Sintering (HFIHS). It enables quick consolidation of powders due to the characteristics of the method, pressure and temperature applied simultaneously [29-32]. However, the effect of these parameters on the microstructure, structure and precipitation kinetics and mechanical properties have not been appropriately evaluated. Thus, the purpose of this study is to figure out how the temperature, time, pressures and heating rates of the two different processing methods, CS and the combination of HFIHS + CS, affect the microstructure, structure and precipitation kinetics in $Al_xCoCrFeMnNi$ HEAs.

2. Materials and Methods

The raw materials employed were Al, Co, Cr, Fe, Mn, and Ni elemental powders with 99.5 % purity and an average particle size of 3-15 μm. A high-energy ball mill Spex 8000M was used to synthesize the $Al_xCoCrFeMnNi$ HEAs with different aluminum concentrations (x = 0.5, 1 and 1.5 at. % - Table 1, composition sintered samples). Milling media and containers were made of hardened steel (D2). Milling conditions were set to: i) 10 h of milling time, ii) powder mass 8.5 g, iii) ball-to-powder ratio of 5:1, iv) argon atmosphere, and v) n-heptane as a process control agent.

The powders were consolidated under two different sintering methods, the conventional sintering method (CS) and the sintering method of induction + conventional (HFIHS + CS):

-The CS method was carried out under the following conditions: the alloyed powders were uniaxially compacted at 1.56 GPa for 10 min. Subsequently, the green samples were sintered at 1200 °C for 3 h with a heating rate of 10 °C/min and a cooling rate of 5 °C/min into a furnace. The resulting sample size was 1x5mm (0.5g).

-The HFIHS + CS method was carried out under the following conditions: the alloyed powders were pressed and pre-sintered under uniaxial compaction of 0.9 GPa at 600 °C for 3 min (HFIHS). The resulting sample size was 1x5mm (0.5g), the induction frequency and power were about 70 kHz and 1.5 kW, respectively, with a heating rate of 150 °C/min and a cooling rate of 40 °C/min under a forced flow of air. The pre-sintering at 600 °C was carried out mainly to retain the nanometric grain size obtained during mechanical alloying and generate an incipient area of contact between particles. Pre-sintering at a minimum heating rate of 150 °C/min is required to generate fast enough thermal expansion rate to be able to break the oxide layer that forms on the surface of the powders, generating a larger contact area between the particles, which accelerates the processes of diffusion [33, 34]. However, high-temperature sintering is necessary to achieve high densification due to the low temperature employed by HFIHS, so additional sintering at 1200 °C for 1 h (CS) with the same heating and cooling conditions was carried out.

The microstructural characterization of the consolidated samples was carried out using a HITACHI SU3500 Scanning Electron Microscope (SEM) and Hitachi HT 7700 Transmission Electron Microscope (TEM). The structural characterization of the consolidated samples was carried out using a Panalytical X'Pert PRO diffractometer and a JEM 2200 FS + CS Transmission Electron Microscope. The x-ray diffraction analysis was performed considering FCC, BCC, BCC ($B2_{ordedered}$), Sigma, M_7C_3, and $M_{23}C_6$ phases using FullProf software [35]. Finally, the hardness and density were evaluated by the LM300 AT microhardness tester and Archimedes method.

3. Results

3.1 Phase decomposition of the solid solution obtained by mechanical alloying during the sintering process

The structural stability in HEAs and its relationship to the physicochemical and thermodynamic properties of the constituent elements are studied using the following parameters: atomic radius difference (δ), enthalpy (ΔH_{mix}) and entropy (ΔS_{mix}) of the mixture and the valence electrons concentration (VEC) [5, 6]. In this sense, the VEC is used to predict the phases present in HEAs due to its simplicity. This parameter can be calculated with the formula of VEC [5, 6]:

$$VEC = \sum_{i=1}^{n} Ci\ (VEC)i$$

Where c_i is the atomic percentage and $(VEC)_i$ is the VEC value for the i element, being 3 for Al, 6 for Cr, 7 for Mn, 8 for Fe, 9 for Co, and 10 for Ni, respectively [5, 6]. According to the valence electron concentration (VEC), the $Al_{0.5}$CoCrFeMnNi and AlCoCrFeMnNi systems should show a BCC phase and FCC phase because the values range from 6.87 to 8. In the $Al_{1.5}$CoCrFeMnNi system, the resulting value was 6.75, so theoretically, a BCC phase should be obtained. The results obtained from the VEC of the HEAs are similar to those reported and calculated by Hu Cheng et al. with the following compositions Al_0, $Al_{0.1}$, $Al_{0.3}$, $Al_{0.5}$, $Al_{0.7,}$ and Al_1 [12].

Fig. 1 and 2 show the XRD patterns obtained from the alloyed powder and the different consolidated systems. The patterns corresponding to alloyed powder show only BCC and FCC phases. However, the consolidated systems show the $B2_{ordered}$, BCC, and FCC phases. In addition to carbides ($M_{23}C_6$ and M_7C_3) and sigma phase. In all systems, the phases resulted agree with those detected by other authors [12-15]. An important aspect is transforming BCC to FCC phase from the alloyed powder to sintered sample in the $Al_{0.5}$CoCrFeMnNi system. In this sense, Wang et al. [36] have reported that aluminum stabilizes the FCC phase when it is less than 11 at. % and it promotes the formation of the BCC phase when it is present in more amount. This phenome is attributed to the phase transition from a metastable state (BCC phase) obtained by the mechanical alloying to a stable state (FCC phase) obtained after sintering.

For the CS and HFIHS + CS methods, the dominant phase (FCC) changes as the concentration of aluminum increases, decreasing the intensity signals and increasing those of the $B2_{ordered}$ and BCC. Making a semi-quantitative analysis for the AlCoCrFeMnNi system sintering by CS method, the phase fraction relation

($B2_{ordered}$ / BCC) is 0.69, and for the $Al_{1.5}$CoCrFeMnNi system, the relation ($B2_{ordered}$ / BCC) is 2.65, an analysis not was carried out for $Al_{0.5}$CoCrFeMnNi system due to low transformed fraction of BCC phase. Small XRD peaks could be associated with the formation of the following carbides: $M_{23}C_6$ when sintering by the CS method and the M_7C_3 carbide for the HFIHS + CS method. The formation of carbides in high-entropy alloys during sintering heat treatment has been reported by several authors [37, 38]. They associate this with carbon's presence in the material caused by the decomposition of the process control agent used in the mechanical alloying stage [38]. This formation is due to the lower number of electrons in the last orbital of each element that generates higher binding energy for the formation of carbides, in addition to the sintering temperature, which promotes diffusion. In the systems studied, the affinity of the elements present to form bonds with carbon is as follows: Al > Cr > Mn > Fe > Co > Ni, due to the high negative values in the Gibbs free energy [39]. In HFIHS + CS methods, the presence of M_7C_3 carbides is observed, which have been reported as non-equilibrium carbides. Their formation is attributed to the rapid heating rate and a short time of sintering treatment. However, for the CS method, the presence of $M_{23}C_6$ equilibrium carbides is observed, which are formed due to long sintering treatment time following the transformation: $M_7C_3 \rightarrow M_{23}C_6$ [40]. Regarding the prediction of phases through the VEC, it is evident that the $Al_{0.5}$CoCrFeMnNi and AlCoCrFeMnNi systems accomplish these predictions, i.e., XRD patterns present the BCC and FCC phases. However, in the $Al_{1.5}$CoCrFeMnNi system, this prediction is not fulfilled since the same phases as the other systems are observed, and the VEC only predicts a BCC phase formation. This behavior can be attributed to the fact that the FCC-BCC region is wider in the $Al_{1.5}$CoCrFeMnNi system than the values calculated by VEC [39].

Fig. 3 shows the backscattered SEM micrographs (SEM - BSE) obtained for the $Al_{0.5}$CoCrFMnNi, AlCoCrFeMnNi and $Al_{1.5}$CoCrFeMnNi systems after sintering by CS and HFIHS + CS methods. Three different phases are present. The first one exhibits light-gray tonality according to XRD patterns (Fig.2); it corresponds to the FCC phase. Its volume fraction decreases as the aluminum content increases, and it transforms into a $B2_{ordered}$ phase of dark-gray tonality, which is consistent with the low atomic weight of aluminum. Finally, precipitates (BCC) are observed within the $B2_{ordered}$ phase, which presents a cuboidal (CS) and plate-like (HFIHS + CS) morphology.

Fig. 4 shows micrographs, elemental mappings, and SAED and NBD patterns obtained by TEM / STEM from the AlCoCrFeMnNi system after sintering by CS and HFIHS + CS methods. This figure confirms the phases $B2_{ordered}$, FCC and BCC mentioned in Fig. 2. The BCC and $B2_{ordered}$ phases reflections have the same interplanar distance. Hence, both signals overlap in XRD. Only the $B2_{ordered}$ phase reflection is observable at 31°, so it is difficult to designate which phase corresponds to the precipitates or the matrix through this technique. However, by the SAED pattern obtained (Fig. 4a), the $B2_{ordered}$ phase is corroborated in the matrix, and the NBD patterns (Fig. 4b) obtained corroborates the BCC phase for the precipitates. Besides, it is observed that the precipitates with cuboidal morphology (CS) have a bimodal size distribution with a length of approximately 500 nm and less than 100 nm, and the precipitates with plate-like morphology (HFIHS + CS) has a size approximately of 2 μm in length. The elements distribution between precipitates and matrix is shown in Fig. 4c. The Co and Mn are distributed homogeneously in precipitates and the matrix. However, chrome and iron are concentrated in the precipitated phase, and Al and Ni are concentrated in the matrix.

3.2 Evolution of Vickers microhardness and density during the sintering process

Fig. 5 shows Vickers microhardness values obtained in the $Al_{0.5}$CoCrFMnNi, AlCoCrFeMnNi, and $Al_{1.5}$CoCrFeMnNi systems after sintering by CS and HFIHS + CS methods. It is observed in this figure that the increase in the aluminum content generates higher hardness values. In addition, the highest values are obtained by the HFIHS method followed by the CS and HFIHS + CS methods.

Fig. 6 shows the density and relative densities of the consolidated samples after sintering by CS, HFIHS, and HFIHS + CS methods. The density values increase for the CS and HFIHS methods compared to the value obtained in the green sample and reach similar values within the error range (~ 80% densification). However, the maximum density is attained for the HFIHS + CS method (~ 95% densification). According to K. A. Khalil et al. [32], the samples sintered using the HFIHS method exhibit higher densification than the CS method. Such behavior is attributed to two factors: an accelerated diffusion process generated by a high-speed heating rate and the constant pressure applied to the material during heating and cooling, which causes a reduction in porosity and higher densification. In addition, a similar trend is observed for the 3

compositions, which indicates that the Al concentration in the systems did not significantly affect the sample's densification.

4. Discussion

The highest densification conditions were observed for the HFIHS + CS method; this behavior is mainly attributed to the simultaneous combination of pressure and temperature during the compaction of the powders. Thus, the 0.9 GPa pressure applied in the HFIHS method during sintering provides an additional driving force for densification, i.e., accelerate internal diffusion processes since it increases the sites and area of contact between particles [29-32]. On the other hand, the effect of temperature on rapid diffusion is mainly due to heating by radiation and conduction applied by electromagnetic waves and heating the compacting die [32, 41, 42].

Due to the increasing addition of aluminum to the CoCrFeMnNi system, two critical transformations occur. The first is that the FCC phase transforms into a mixture of FCC and $B2_{ordered}$ phases. The increase in aluminum generates a change from the FCC phase to the $B2_{ordered}$ phase. This is attributed to the BCC structure generally having a lower atomic packing density (68%) than the FCC and HCP structures (both 74%) and therefore can more easily accommodate larger solute atoms like Al=1.43 Å (Co = 1.251, Cr = 1.249, Fe = 1.241, Mn = 1.350 Ni = 1.246 Å) [12]. Besides, the excessive addition of aluminum changes the FCC phase to a compact $B2_{ordered}$ phase due to a large lattice distortion energy that destabilizes the FCC structure [22, 43].

Regarding the second transformation, the BCC phase precipitates from the $B2_{ordered}$ phase due to the high number of aluminum atoms that incorporate into the crystalline lattice, which take random atomic positions within the ordered structure, excluding the other elements. In addition, other thermodynamic aspects such as negative enthalpy values of the mixture of Cr-Fe (-7 kJ mol^{-1}) and the affinity between elements induce the formation of BCC phase precipitates [14, 44, 45]. The difference between the $B2_{ordered}$ and BCC phases is attributed to the periodicity of the arrangement of atoms in the unit cell [46]. The $B2_{ordered}$ phase is rich in Al, Ni, Mn, and Co, and the atoms have a preferential occupation in the atomic sites (000) and/or (1/2 1/2

1/2). According to the similar atomic radii and electronegativity values between Co, Ni, Mn, and Fe, these elements must occupy one of the mentioned sites, while Al and Cr are located in the other available sites [46, 47]. On the other hand, in the BCC phase, Al, Ni, Co, Mn, and Fe can occupy any atomic site in the lattice.

Sutanuka Mohanty et al. [48] mention that it is possible to obtain precipitates in a sintering process from the supersaturated solid solution (i. e., atomization is a rapid solidification technique and therefore promotes solid solution) obtained through mechanical alloying in HEA. In this sense, the precipitation mechanism proposed in some HEA with Al is spinodal decomposition due to a miscibility gap in these systems [49-52]. The cuboidal morphology of the precipitates observed by the CS method is attributed to moderate lattice distortion between matrix/precipitate [16, 18, 51]. Besides, V. Soni et al. [49] mentions that a temperature of 600 °C is sufficient to form the BCC phase with a cubic morphology. In addition, there are generally two main mechanisms to decrease the surface energy of the system: coarsening and coalescence. In this regard, coarsening occurs when the interfacial energy is reduced through a mass transfer process by diffusion from high interfacial energy precipitates to low interfacial energy precipitates, significantly altering their morphology [53-56]. This energy minimization leads to the growth of larger particles at the expense of smaller particles. Thus, the average size of the precipitates must increase with time, and the number of these must decrease, i.e., the change in morphology occurs due to the small particles dissolving and transferring their mass to the larger particles, which is corroborated by the observed bimodal distribution. On the other hand, the union between two precipitates due to the overlap of their interdifusional zones (coalescence) is also observed (Fig 4 b.) [53-56].

On the other hand, the morphology observed by the HFIHS + CS method can be attributed to a more complex phenomenon due to the speed of diffusion provided by the HFIHS method, i.e., application of induction heating significantly increases the heating rates. This behavior is due to the high frequency of electromagnetic waves that cause more significant vibration in the atoms within the lattice [57].

A possible explanation for this phenomenon is that the chrome of the $B2_{ordered}$ phase enriches the BCC phase due to the low solubility of Cr with Al and Ni [58]. Therefore, the high diffusion speed in the HFIHS

method and the time and temperature of sintering by the CS method generate a faster coarsening in the cuboidal precipitates, which results in coarse elongated plate-like precipitates. V. Soni et al. [49] mention that the growth of precipitates occurs in the soft directions (preferential orientations) of the crystal lattice due to the coarsening of the microstructures depending to a great extent on the interaction between the interfacial and elastic energies.

The changes in microstructure with the increasing addition of aluminum affect the Vickers hardness (HV), which is attributed to the transformation from the FCC phase to the $B2_{ordered}$ phase (Fig.2). In addition, the low HV values obtained in the CS and HFIHS + CS methods are related to the coarsening of the BCC precipitates. The CS method is at an initial coarsening stage, and the HFIHS + CS method is at a more advanced coarsening stage. The high value in HV by the HFIHS pre-sintered method is attributed to an initial stage for the phase separation (the initial stage of precipitate formation) and small grain size, which was retained in the pre-sintered method.

4. Conclusions

The BCC phase precipitated in $Al_{0.5}CoCrFeMnNi$, AlCoCrFeMnNi, and $Al_{1.5}CoCrFeMnNi$ systems show morphological changes associated with different coarsening kinetics that affect the hardness. The different diffusion rates between sintering methods induce two different morphologies in the BCC phase, cuboidal and plate-like. Cuboidal morphology is observed in the CS method due to slow diffusion, while for the HFIHS + CS method, the higher diffusion results in a plate-like morphology. Concerning behavior Vickers microhardness, the high value obtained by the HFIHS pre-sintered method is attributed to an initial stage of precipitate formation and nanometric grain size, which was retained in the pre-sintered method. The low values obtained by the HFIHS + CS method are attributed to the high coarsening kinetics. In addition, two types of carbides ($M_{23}C_6$ and M_7C_3) are observed. The $M_{23}C_6$ carbide is identified in systems sintered by the CS method, and the M_7C_3 carbide is identified in systems sintered by the HFIHS+ CS method. Finally, the sintering method of HFIHS + CS exhibited higher-level densification (~95%) than the CS method (~80%).

Acknowledgments

The scholarship under grant No. 715550 provided by CONACYT is duly recognized. Authors gratefully thank K. Campos-Venegas, R. A. Ochoa-Gamboa, and C. E. Ornelas-Gutierrez for their valuable technical support throughout the study.

References

[1] V. Shivam, J. Basu, R. Manna, Local Composition Migration Induced Microstructural Evolution and Mechanical Properties of Non-equiatomic $Fe_{40}Cr_{25}Ni_{15}Al_{15}Co_5$ Medium-Entropy Alloy, Metall Mater Trans A. 52 (2021) 1777–1789. https://doi.org/10.1007/s11661-021-06188-7

[2] E. J. Pickering, N. G. Jones, High-entropy alloys: a critical assessment of their founding principles and future prospects, International Materials Reviews. 61:3 (2016) 183-202. https://doi.org/10.1080/09506608.2016.1180020

[3] Y. Zhang, T.T. Zuo, Z. Tang, M.C. Gao, K.A. Dahmen, P.K. Liaw, Z.P. Lu, Microstructures and properties of high-entropy alloys. Progress in Materials Science, 61 (2014) 1-93. https://doi.org/10.1016/j.pmatsci.2013.10.00

[4] J.W. Yeh, Alloy Design Strategies and Future Trends in High-Entropy Alloys. JOM. 65 (2013) 1759–1771. https://doi.org/10.1007/s11837-013-0761-6

[5] S. Guo, C. Ng, J. Lu, C. T. Liu, Effect of valence electron concentration on stability of FCC or BCC phase in high entropy alloys, Journal of Applied Physics. 109 (2010) 103505. https://doi.org/10.1063/1.3587228

[6] S. Guo, C.T. Liu, Phase stability in high entropy alloys: Formation of solid-solution phase or amorphous phase, Progress in Natural Science: Materials International. 21 (2011) 433-446. https://doi.org/10.1016/S1002-0071(12)60080-X

[7] F. Otto, Y. Yang, H. Bei, E.P. George, Relative effects of enthalpy and entropy on the phase stability of equiatomic high-entropy alloys, Acta Materialia. 61:7 (2013) 2628-2638, https://doi.org/10.1016/j.actamat.2013.01.042

[8] A.S. Sharma, S. Yadav, K. Biswas, B. Basu, High-entropy alloys and metallic nanocomposites: Processing challenges, microstructure development and property enhancement, Materials Science and Engineering: R: Reports. 131 (2018) 1-42. https://doi.org/10.1016/j.mser.2018.04.003

[9] D.B. Miracle, O.N. Senkov, A critical review of high entropy alloys and related concepts, Acta Materialia. 122 (2017) 448–511. https://doi.org/10.1016/j.actamat.2016.08.081

[10] J. Chen, X. Zhou, W. Wang, B. Liu, Y. Lv, W. Yang, D. Xu, Y. Liu, A review on fundamental of high entropy alloys with promising high–temperature properties, Journal of Alloys and Compounds. 760 (2018) 15-30. https://doi.org/10.1016/j.jallcom.2018.05.067

[11] B. Cantor, I.T.H. Chang, P. Knight, A.J.B.Vincent, Microstructural development in equiatomic multicomponent alloys, Materials Science and Engineering. 375–377 (2004) 213-218. https://doi.org/10.1016/j.msea.2003.10.257.

[12] H. Cheng, X. Liu, Q. Tang, W. Wang, X. Yan, P. Dai, Microstructure and mechanical properties of $FeCoCrNiMnAl_x$ high-entropy alloys prepared by mechanical alloying and hot-pressed sintering, Journal of Alloys and Compounds. 775 (2019) 742-751. https://doi.org/10.1016/j.jallcom.2018.10.168

[13] J.Y. He, W.H. Liu, H. Wang, Y. Wu, X.J. Liu, T.G. Nieh, Z.P. Lu, Effects of Al addition on structural evolution and tensile properties of the FeCoNiCrMn high-entropy alloy system, Acta Materialia. 62 (2014) 105-113. https://doi.org/10.1016/j.actamat.2013.09.037

[14] V. Shivam, J. Basu, Y. Shadangi, M.K. Singh, N.K. Mukhopadhyay, Mechano-chemical synthesis, thermal stability and phase evolution in AlCoCrFeNiMn high entropy alloy, Journal of Alloys and Compounds. 757 (2018) 87-97. https://doi.org/10.1016/j.jallcom.2018.05.057

[15] R.M. Pohan, B. Gwalani, J. Lee, T. Alam, J.Y. Hwang, H.J. Ryu, R. Banerjee, S.H Hong, Microstructures and mechanical properties of mechanically alloyed and spark plasma sintered

$Al_{0.3}$CoCrFeMnNi high entropy alloy, Materials Chemistry and Physics. 210 (2018) 62-70. https://doi.org/10.1016/j.matchempys.2017.09.013

[16] Y. Ma, Q. Wang, B.B. Jiang, C.L. Li, J.M. Hao, X.N. Li, C. Dong, T.G. Nieh, Controlled formation of coherent cuboidal nanoprecipitates in body-centered cubic high-entropy alloys based on $Al_2(Ni,Co,Fe,Cr)_{14}$ compositions, Acta Materialia. 147 (2018) 213-225. https://doi.org/10.1016/j.actamat.2018.01.050

[17] J. Hao, Y. Ma, Q. Wang, C. Zhang, C. Li, C. Dong, Q. Song, P.K. Liaw, Formation of cuboidal B2 nanoprecipitates and microstructural evolution in the body-centered-cubic $Al_{0.7}NiCoFe_{1.5}Cr_{1.5}$ high-entropy alloy, Journal of Alloys and Compounds. 780 (2019) 408-421. https://doi.org/10.1016/j.jallcom.2018.11.381

[18] Y. Ma, B. Jiang, C. Li, Q. Wang, C. Dong, P.K. Liaw, F. Xu, L. Sun, The BCC/B2 Morphologies in Al_xNiCoFeCr High-Entropy Alloys, Metals. 7:2 (2017) 57. https://doi.org/10.3390/met7020057

[19] D.G. Shaysultanov, G.A. Salishchev, Yu.V. Ivanisenko, S.V. Zherebtsov, M.A. Tikhonovsky, N.D. Stepanov, Novel $Fe_{36}Mn_{21}Cr_{18}Ni_{15}Al_{10}$ high entropy alloy with bcc/B2 dual-phase structure, Journal of Alloys and Compounds. 705 (2017) 756-763. https://doi.org/10.1016/j.jallcom.2017.02.211

[20] A. Munitz, S. Salhov, S. Hayun, N. Frage, Heat treatment impacts the micro-structure and mechanical properties of AlCoCrFeNi high entropy alloy, Journal of Alloys and Compounds. 683 (2016) 221-230 https://doi.org/10.1016/j.jallcom.2016.05.034

[21] V. Shivam, J. Basu, V.K. Pandey, Y. Shadangi, N.K. Mukhopadhyay, Alloying behaviour, thermal stability and phase evolution in quinary AlCoCrFeNi high entropy alloy, Advanced Powder Technology. 29:9 (2018) 2221-2230. https://doi.org/10.1016/j.apt.2018.06.006

[22] W.R. Wang, W.L. Wang, S.C. Wang, Y.C. Tsai, C.H. Lai, J.W. Yeh, Effects of Al addition on the microstructure and mechanical property of Al_xCoCrFeNi high-entropy alloys, Intermetallics. 26 (2012) 44-51. https://doi.org/10.1016/j.intermet.2012.03.005

[23] C.M. Lin, H.L. Tsai, Evolution of microstructure, hardness, and corrosion properties of high-entropy $Al_{0.5}$CoCrFeNi alloy, Intermetallics. 19:3 (2011) 288-294. https://doi.org/10.1016/j.intermet.2010.10.008

[24] J. Joseph, P. Hodgson, & T. Jarvis, X. Wu, N. Stanford, D. Fabijanic, Effect of hot isostatic pressing on the microstructure and mechanical properties of additive manufactured $Al_xCoCrFeNi$ high entropy alloys, Materials Science and Engineering: A. 733 (2018) 59-70. https://doi:10.1016/j.msea.2018.07.036

[25] W. Ji, W. Wang, H. Wang, J. Zhang, Y. Wang, F. Zhang, Z. Fu, Alloying behavior and novel properties of CoCrFeNiMn high entropy alloy fabricated by mechanical alloying and spark plasma sintering, Intermetallics. 56 (2015) 24-27. https://doi.org/10.1016/j.intermet.2014.08.008

[26] H. Khanchandani, P. Sharma, R. Kumar, O. Maulik, V. Kumar, Effect of sintering on phase evolution in $AlMgFeCuCrNi_{4.75}$ high entropy alloy, Advanced Powder Technology. 27 (2016) 289–294. https://doi.org/10.1016/j.apt.2016.01.001

[27] S. Praveen, B.S. Murty, R.S. Kottada, Phase Evolution and Densification Behavior of Nanocrystalline Multicomponent High Entropy Alloys During Spark Plasma Sintering, JOM. 65 (2013) 1797–1804. https://doi.org/10.1007/s11837-013-0759-0

[28] R. B. Mane, Y. Rajkumar, B. B. Panigrahi, Sintering mechanism of CoCrFeMnNi high-entropy alloy powders, Powder Metallurgy. 61 (2018) 131–138. https://doi.org/10.1080/00325899.2018.1433268

[29] H. S. Kang, H. Kwon, I.J Shon, Rapid Consolidation and Mechanical Properties of Binderless Nanostructured (W,Ti)C by High-Frequency Induction Heating, Materials Transactions. 54 (2013) 2301-2304. https://doi.org/10.2320/matertrans.M2013273

[30] H. C. Kim, J. K. Yoon, J. M. Doh, I. Y. Ko, I. J. Shon, Rapid sintering process and mechanical properties of binder less ultra fine tungsten carbide, Materials Science and Engineering: A. 435–436 (2006) 717-724. https://10.1016/j.msea.2006.07.127

[31] H. C. Kim, I. J. Shon, I. K. Jeong, I. Y. Ko, J. K. Yoon, J. M. Doh, Rapid sintering of ultra fine WC and WC-Co hard materials by high-frequency induction heated sintering and their mechanical properties, Metals and Materials International. 13 (2007) 39–45. https://doi.org/10.1007/BF03027821

[32] K.A. Khalil, A.A. Almajid, Effect of high-frequency induction heat sintering conditions on the microstructure and mechanical properties of nanostructured magnesium/hydroxyapatite nanocomposites, Materials and Design. 36 (2012) 58–68. https://doi:10.1016/j.matdes.2011.11.008

[33] J.M. Mendoza-Duarte, F.C. Robles-Hernandez, E. Rocha-Rangel, Y. Todaka, N. Adachi, I. Estrada-Guel, C. G. Garay-Reyes, M. A. Ruiz Esparza-Rodríguez, R. Martínez-Sánchez, Increase of the mechanical response of pure aluminum by grain refinement retained with an alternative rapid sintering route. Journal of Materials Research. 36 (2021) 1328–1340. https://doi.org/10.1557/s43578-021-00176-8

[34] S. Raynova, Y. Collas, F. Yang, L. Bolzoni, Advancement in the Pressureless Sintering of CP Titanium Using High-Frequency Induction Heating, Metallurgical and Materials Transactions A. 50 (2019) 4732–4742. https://doi.org/10.1007/s11661-019-05381-z

[35] J. Rodriguez-Carvajal, Recent advances in magnetic structure determination by neutron powder diffraction, Physica B: Condensed Matter. 192:1-2 (1993) 55-69. https://doi.org/10.1016/0921-4526(93)90108-I

[36] C. Wang, W. Ji, Z. Fu, Mechanical alloying and spark plasma sintering of CoCrFeNiMnAl high-entropy alloy, Advanced Powder Technology. 25:4 (2014) 1334-1338. https://doi.org/10.1016/j.apt.2014.03.014

[37] I. Moravcik, A. Kubicek, L. Moravcikova-Gouvea, O. Adam, V. Kana, V. Pouchly, A. Zadera, I. Dlouhy, The Origins of High-Entropy Alloy Contamination Induced by Mechanical Alloying and Sintering, Metals. 10:9 (2020) 1186. https://doi.org/10.3390/met10091186

[38] P. Wang, H. Cai, S. Zhou, L. Xu, Processing, microstructure and properties of $Ni_{1.5}CoCuFeCr_{0.5-x}V_x$ high entropy alloys with carbon introduced from process control agent, Journal of Alloys and Compounds. 695 (2017) 462-475. https://doi.org/10.1016/j.jallcom.2016.10.288

[39] M.A. Ruiz-Esparza-Rodríguez, C.G. Garay-Reyes, I. Estrada-Guel, J.L. Hernández-Rivera, J.J. Cruz-Rivera, E. Gutiérrez-Castañeda, C.D. Gómez-Esparza, R. Martínez-Sánchez, Influence of process control agent and Al concentration on synthesis and phase stability of a mechanically alloyed $Al_xCoCrFeMnNi$

high-entropy alloy, Journal of Alloys and Compounds. 882 (2021) 160770. https://doi.org/10.1016/j.jallcom.2021.160770

[40] K. Wieczerzak, P. Bala, R. Dziurka, T. Tokarski, G. Cios, T. Koziel, L. Gondek, The effect of temperature on the evolution of eutectic carbides and $M_7C_3 \rightarrow M_{23}C_6$ carbides reaction in the rapidly solidified Fe-Cr-C alloy, Journal of Alloys and Compounds. 698 (2017) 673-684. https://doi.org/10.1016/j.jallcom.2016.12.252

[41] M. Dewidar, Microstructure and mechanical properties of biocompatible high density Ti–6Al–4V/W produced by high frequency induction heating sintering, Materials & Design. 31 (2010) 3964-3970. https://doi.org/10.1016/j.matdes.2010.03.042

[42] S.W Kim, K.A Khalil, High-Frequency Induction Heat Sintering of Mechanically Alloyed Alumina-Yttria-Stabilized Zirconia Nano-Bioceramics, Journal of the American Ceramic Society. 89 (4), (2006) 1280–1285. https://doi.org/10.1111/j.1551-2916.2005.00902.x

[43] K. Zhang, Z. Fu, Effects of annealing treatment on phase composition and microstructure of $CoCrFeNiTiAl_x$ high-entropy alloys, Intermetallics. 22 (2012) 24-32. https://doi.org/10.1016/j.intermet.2011.10.010

[44] A. Manzoni, H. Daoud, & R. Völkl, U. Glatzel, N. Wanderka, Phase separation in equiatomic AlCoCrFeNi high-entropy alloy, Ultramicroscopy. 132 (2013) 212-215. https://doi.org/10.1016/j.ultramic.2012.12.015

[45] S. Singh, N. Wanderka, B.S. Murty, U. Glatzel, J. Banhart, Decomposition in multicomponent AlCoCrCuFeNi high-entropy alloy, Acta Materialia. 59 (2011) 182–190. https://doi.org/10.1016/j.actamat.2010.09.023

[46] L. Meshi, Y. Linden, A. Munitz, S. Salhov, M. Pinkas, Retardation of the σ phase formation in the AlCoCrFeNi multi-component alloy, Materials Characterization. 148 (2019) 171-177. https://doi.org/10.1016/j.matchar.2018.12.010

[47] S. Xie, R. Li, T. Yuan, L. Zhou, M. Zhang, M. Wang, P. Niu, P. Cao, C. Chen, Effect of heating rate on microstructure and mechanical properties of AlCoCrFeNi high entropy alloy produced by spark plasma sintering, Materials Characterization. 154 (2019) 169-180, https://doi.org/10.1016/j.matchar.2019.05.022

[48] S. Mohanty, N.P. Gurao, K. Biswas, Sinter ageing of equiatomic $Al_{20}Co_{20}Cu_{20}Zn_{20}Ni_{20}$ high entropy alloy via mechanical alloying, Materials Science and Engineering: A. 617 (2014) 211-218. https://doi.org/10.1016/j.msea.2014.08.046

[49] V. Soni, B. Gwalani, T. Alam, S. Dasari, Y. Zheng, O.N. Senkov, D. Miracle, R. Banerjee, Phase inversion in a two-phase, BCC+B2, refractory high entropy alloy, Acta Materialia. 185 (2020) 89-97. https://doi.org/10.1016/j.actamat.2019.12.004

[50] Z. Tang, O.N. Senkov, C.M. Parish, C. Zhang, F. Zhang, L.J. Santodonato, G. Wang, G. Zhao, F. Yang, P.K. Liaw, Tensile ductility of an AlCoCrFeNi multi-phase high-entropy alloy through hot isostatic pressing (HIP) and homogenization, Materials Science and Engineering: A. 647 (2015) 229-240. https://doi.org/10.1016/j.msea.2015.08.078

[51] Q. Tian, G. Zhang, K. Yin, W. Wang, W. Cheng, Y. Wang, The strengthening effects of relatively lightweight AlCoCrFeNi high entropy alloy, Materials Characterization. 151 (2019) 302-309. https://doi.org/10.1016/j.matchar.2019.03.006

[52] L.J. Zhang, K. Guo, H. Tang, M.D. Zhang, J.T. Fan, P. Cui, Y.M. Ma, P.F. Yu, G. Li, The microstructure and mechanical properties of novel Al-Cr-Fe-Mn-Ni high-entropy alloys with trimodal distributions of coherent B2 precipitates, Materials Science and Engineering: A. 757 (2019) 160-171. https://doi.org/10.1016/j.msea.2019.04.104

[53] A. Baldan, Review Progress in Ostwald ripening theories and their applications to nickel-base superalloys Part I: Ostwald ripening theories, Journal of Materials Science. 37 (2002) 2171–2202. https://doi.org/10.1023/A:1015388912729

[54] Z. Mao, C.K. Sudbrack, K.E Yoon, G. Martin, D.N. Seidman, The mechanism of morphogenesis in a phase-separating concentrated multicomponent alloy. Nature Mater. 6 (2007) 210–216. https://doi.org/10.1038/nmat1845

[55] F. Masoumi, M. Jahazi, D. Shahriari, J. Cormier, Coarsening and dissolution of γ′ precipitates during solution treatment of AD730™ Ni-based superalloy: Mechanisms and kinetics models, Journal of Alloys and Compounds. 658 (2016) 981-995. https://doi.org/10.1016/j.jallcom.2015.11.002

[56] N. Mrozowski, G. Hénaff, F. Hamon, A.L. Rouffié, J.M. Franchet, J. Cormier, P. Villechaise, Aging of γ′ Precipitates at 750 °C in the Nickel-Based Superalloy AD730™: A Thermally or Thermo-Mechanically Controlled Process Metals. 10(4) 426 (2020) 1-19. https://doi.org/10.3390/met10040426

[57] K. Zyguła, M. Wojtaszek, T. Śleboda, S. Lech, O. Lypchanskyi, G. Korpała, U. Prahl, The Influence of Induction Sintering on Microstructure and Deformation Behavior of Ti-5Al-5Mo-5V-3Cr Alloy, Metall Mater Trans A. 52 (2021) 1699–1713. https://doi.org/10.1007/s11661-021-06179-8

[58] N.G. Jones, A. Frezza, H.J. Stone, Phase equilibria of an $Al_{0.5}$CrFeCoNiCu High Entropy Alloy, Materials Science and Engineering: A. 615 (2014) 214-221. https://doi.org/10.1016/j.msea.2014.07.059

Figure Captions

Fig. 1 Diffractograms obtained from the alloyed powder corresponding to the systems $Al_{0.5}$CoCrFeMnNi, AlCoCrFeMnNi and $Al_{1.5}$CoCrFeMnNi.

Fig. 2 Diffractograms obtained from the systems $Al_{0.5}$CoCrFeMnNi, AlCoCrFeMnNi and $Al_{1.5}$CoCrFeMnNi after sintering by CS and HFHIS + CS methods.

Fig. 3 Micrographs (SEM-BSE) from the systems $Al_{0.5}$CoCrFeMnNi, AlCoCrFeMnNi and $Al_{1.5}$CoCrFeMnNi in samples sintered using (a) CS and (b) HFHIS + CS methods.

Fig. 4 Micrographs, elemental mappings, and SAED and NBD patterns obtained by TEM/STEM from the AlCoCrFeMnNi system after sintering by CS and HFHIS + CS methods.

Fig. 5 Vickers Microhardness obtained from the systems $Al_{0.5}$CoCrFeMnNi, AlCoCrFeMnNi and $Al_{1.5}$CoCrFeMnNi after sintering by CS, HFIHS and HFIHS + CS methods.

Fig.6 Density and densification (%) obtained in green, and after conventional sintering (CS), high-frequency Induction heat sintering (HFIHS), and high-frequency Induction heat +conventional sintering (HFIHS + CS) in the different systems.

Fig 1

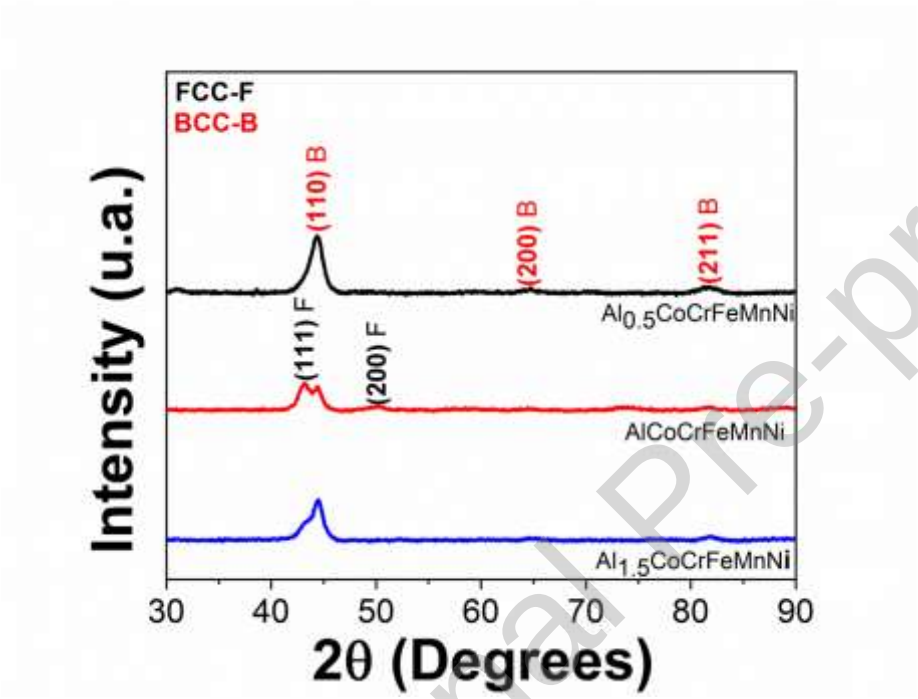

Fig 2

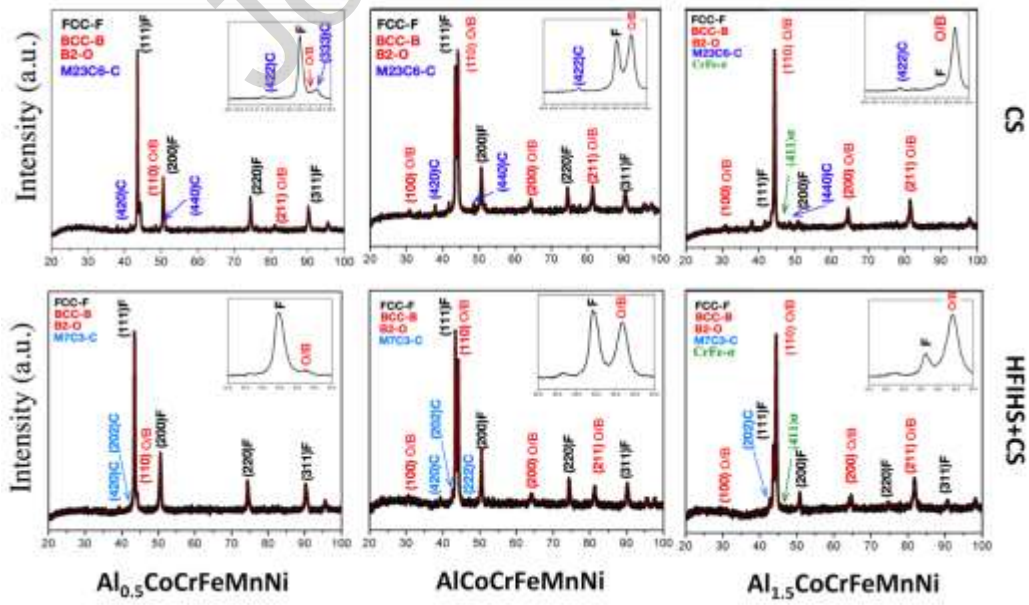

Fig 3

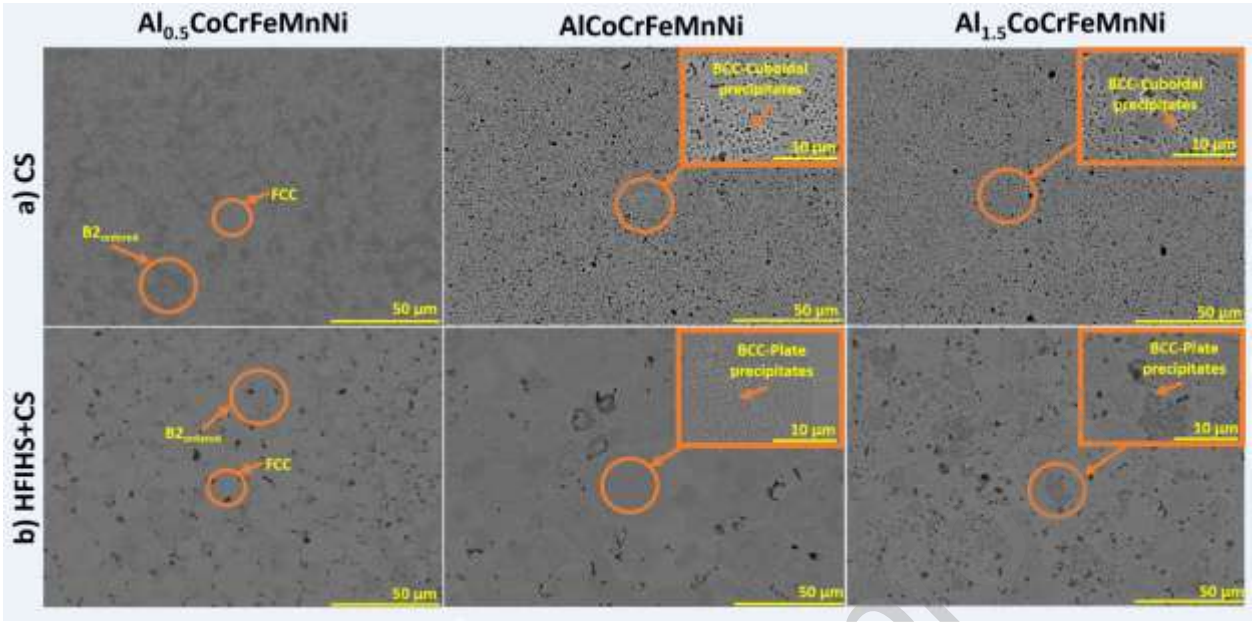

Fig 4

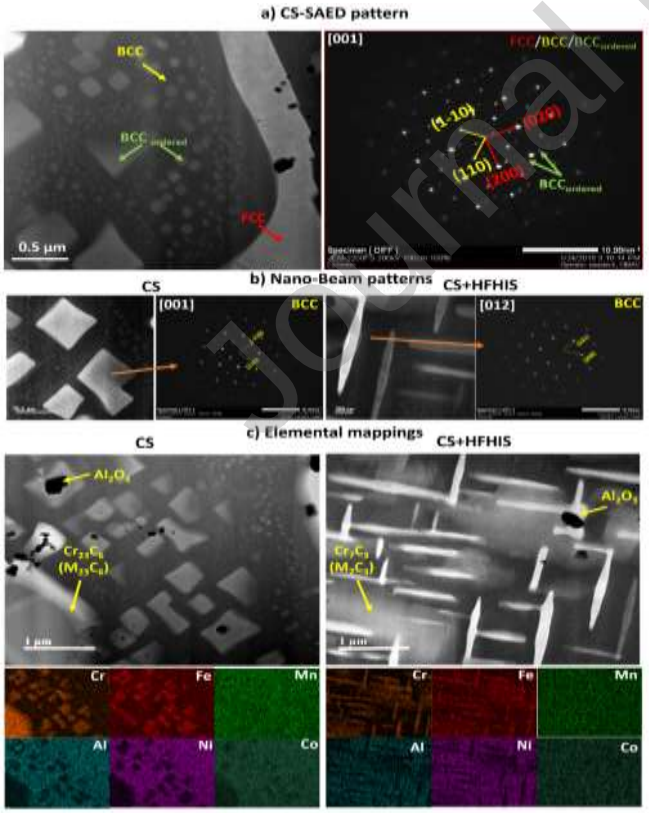

Fig 5

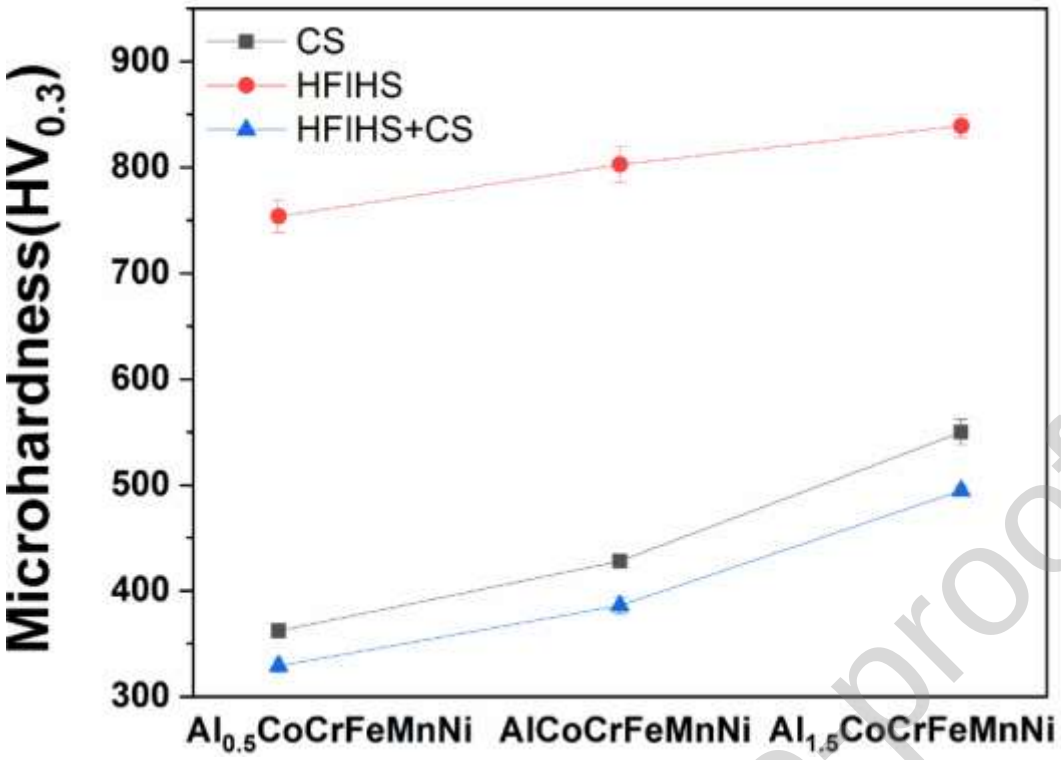

Fig 6

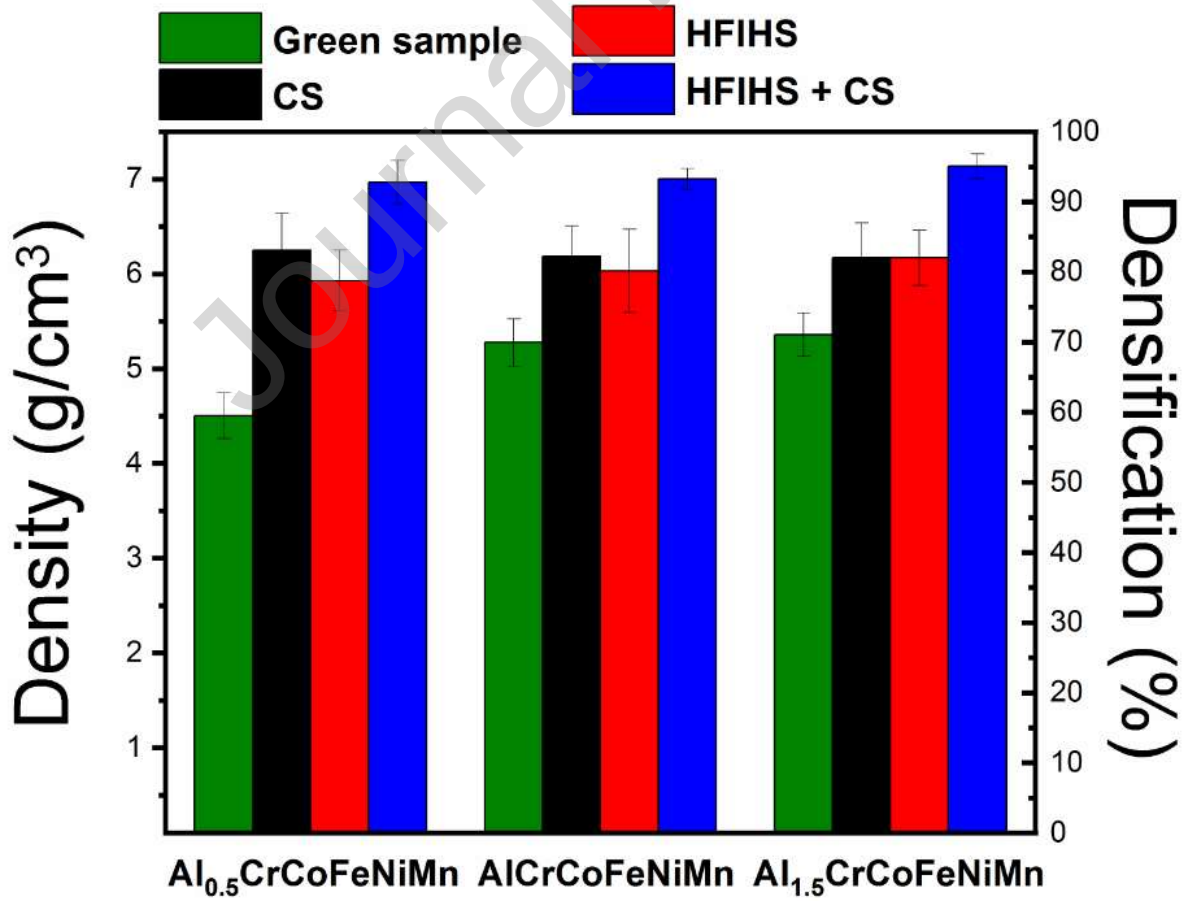

Table. 1 Composition (at. %) obtained by SEM-EDS analysis of $Al_{0.5}$CrCoFeMnNi, AlCrCoFeMnNi, and $Al_{1.5}$CrCoFeMnNi systems after sintering.

	Composition (at %)											
System	***Al***	**±**	***Co***	**±**	***Cr***	**±**	***Fe***	**±**	***Mn***	**±**	***Ni***	**±**
Al0.5CoCrFeMnNi	9.3	0.1	18.3	0.2	18.5	0.2	18.3	0.2	18.6	0.2	17	0.1
AlCoCrFeMnNi	16.3	0.1	16.5	0.1	16.8	0.2	16.5	0.1	16.9	0.2	17	0.1
Al1.5CoCrFeMnNi	23.98	0.1	15.3	0.2	14.1	0.1	15.7	0.2	15.6	0.2	14.6	0.2

±= Standard error.

CRediT authorship contribution statement

M.A. Ruiz-Esparza-Rodriguez: Methodology, Validation, Formal analysis, Investigation, Writing - Original Draft, Visualization. **C.G. Garay-Reyes**: Conceptualization, Visualization, Writing - Review & Editing, Supervision, Project administration. **J.L. Hernández-Rivera**: Formal analysis. **I. Estrada-Gue**l: Methodology, Formal analysis, Conceptualization**. J.J. Cruz-Rivera:** Formal analysis. **E. Gutiérrez-Castañeda**: Formal analysis. **J.M. Mendoza-Duarte**: Formal analysis. **S. González**: Formal analysis. **R. Martínez-Sánchez**: Conceptualization, Visualization, Writing - Review & Editing, Supervision.

Declaration of Competing Interest

☒ The authors declare that they have no known competing financial interests or personal relationships that could have appeared to influence the work reported in this paper.

☐The authors declare the following financial interests/personal relationships which may be considered as potential competing interests:

Highlights

- $Al_xCoCrFeMnNi$ (x= 0.5, 1 and 1.5 at. %) HEAs present $B2_{ordered}$ and FCC phases
- BCC phase precipitates from $B2_{ordered}$ phase in Al_x (x=1 and 1.5 at. %)
- Precipitates (BCC) with cuboidal and plate-like morphology are observed
- The coarsening kinetics of the BCC phase is dependent on the sintering method
- The HFIHS + CS achieves higher densification than the CS and HFIHS alone